Polar Magnetic Oxides

DOI: 10.1002/anie.200((will be filled in by the editorial staff))

Polar and Magnetic Mn_2FeMO_6 (M = Nb, Ta) with $LiNbO_3$-type Structure - High Pressure Synthesis**

*Man-Rong Li, David Walker, Maria Retuerto, Tapati Sarkar, Joke Hadermann, Peter W. Stephens, Mark Croft, Alexander Ignatov, Christoph P. Grams, Joachim Hemberger, Israel Nowik, P. Shiv Halasyamani, T. Thao Tran, Swarnakamal Mukherjee, Tanusri Saha Dasgupta, Martha Greenblatt**

Polar oxides are of much interest in materials science and engineering. Their symmetry-dependent properties such as ferroelectricity/multiferroics, piezoelectricity, pyroelectricity, and second-order harmonic generation (SHG) effect are important for technological applications.[1] However, polar crystal design and synthesis is challenging, because multiple effects, such as steric or dipole-dipole interactions, typically combine to form non-polar structures; so the number of known polar materials, especially polar magnetoelectric materials, is still severely restricted.[2] Therefore, it is necessary for the material science community to develop new strategies to create these materials.

[*] Dr. M.R. Li, M. Retuerto, T. Sarkar, M. Greenblatt
Department of Chemistry and Chemical Biology
Rutgers, The State University of New Jersey
610 Taylor Road, Piscataway, NJ 08854 (USA)
E-mail: martha@rutchem.rutgers.edu

Dr. D. Walker
Lamont-Doherty Earth Observatory, Columbia University
61 Route 9W-PO Box 1000, Palisades, NY 10964 (USA)

Dr. J. Hadermann
EMAT, University of Antwerp
Groenenborgerlaan 171, B-2020 Antwerp (Belgium)

Dr. P. W. Stephens
Department of Physics & Astronomy
State University of New York
Stony Brook, NY 11794 (USA)

Dr. M. Croft, A. Ignatov
Department of Physics & Astronomy
Rutgers, The State University of New Jersey
136 Frelinghuysen Road, Piscataway, Nj 08854 (USA)

Dr. C. P. Grams, J. Hemberger
II. Physikalisches Institut, Universität zu Köln
D-50937 Köln (Germany)

Dr. I. Nowik
Racah Institute of Physics
Hebrew University, Jerusalem, 91904 (Israel)

Dr. P.S. Halasyamani, T. T. Tran
Department of Chemistry, University of Houston
136 Fleming Building, Houston, TX 77204 (USA)

Dr. S. Mukherjee, Dr. T. S. Dasgupta
Department of Condensed Matter Physics and Materials Sciences, S. N. Bose National Centre for Basic Sciences
JD Block, Sector III, Salt Late, Kolkata 700098 (India)

[**] This work was supported by the NSF-DMR-0966829 grant, Rutgers University (Board of Governor Professor Grant), and the DOD-VV911NF-12-1-0172 grant. Use of the National Synchrotron Light Source, Brookhaven National Laboratory was supported by the DOE BES (DE-AC02-98CH10886). PSH and TTT thank the Welch Foundation (Grant E-1457) for support.

Supporting information for this article is available on the WWW under http://www.angewandte.org or from the author

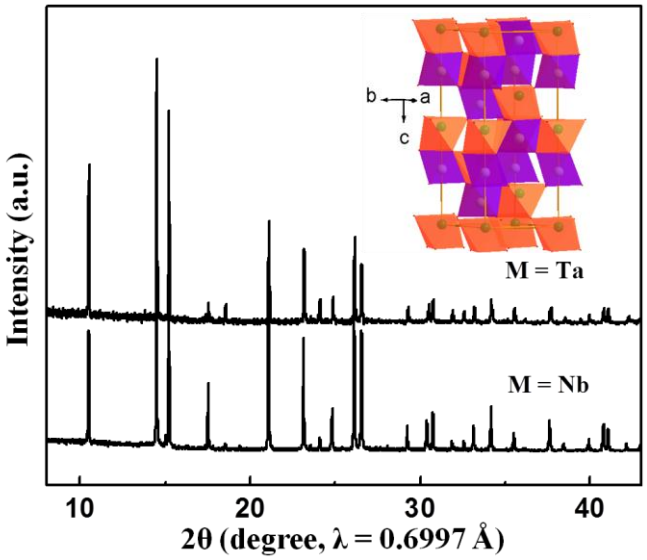

Figure 1. Powder SXRD patterns of Mn_2FeMO_6 (M = Nb (bottom) and Ta (top)). Inset shows the LN-type unit cell crystal structure of Mn_2FeMO_6, where Mn is located at A-site, Fe/M disordered over B-site. MnO_6 octahedra, orange; $(Fe/M)O_6$ octahedra, blue.

Recently, exotic ABO_3-type perovskites with unusually small A-site cations have attracted much attention due to the formation of $LiNbO_3$ (LN)-type polar structure at high pressure (HP) (Section 1 in Supporting Information (SI)).[3] So far, several LN-type ABO_3 oxides have been discovered as metastable quenched phases, including $ZnSnO_3$[4a], $CdPbO_3$[4b], $(In_{1-x}\square_x)MO_{3-\delta}$ (M = Mn/Fe, □ = vacancy)[5], $ScFeO_3$[3b], and the high pressure polymorphs of $MnMO_3$ (M = Ti, Sn)[6] and $FeTiO_3$[7], which show either SHG[4] or (near) room temperature (RT) multiferroic behavior.[3,5-7] Compared with the research in HP-stabilized LN-type ABO_3 oxides, there are few studies of systems with multiple B-site cations, such as $A_2BB'O_6$, containing small A-ions. Occupation of the octahedral B sublattice by two or more different cations can generate interesting physical properties such as magnetoresistance.[8] To the best of our knowledge, to date, only Mn_2BSbO_6 (B = Fe, V, Cr, Ga, Al) with a small A (Mn^{2+}) and mixed B-site cations have been stabilized under HP.[9,10] Among the Mn_2BSbO_6 HP phases, Mn_2FeSbO_6 is potentially the most interesting, as it displays a sharp magnetic transition around 270 K, due to the magnetic interactions of $Mn^{+2}(d^5)$ and Fe^{+3} (d^5); however, it adopts a hexagonal centrosymmetric ilmenite (IL) structure. In this work, we present the polar LN-type magnetic oxides Mn_2FeMO_6 (M = Nb, Ta) in the $A_2BB'O_6$ family via HP synthesis, and investigate their crystal structures, formal oxidation states, magnetic properties, SHG effect, and dielectric properties. Theoretical calculations within the framework of density functional theory (DFT)

supplemented with Coulomb interaction, U, were also carried out to provide theoretical verification of the experimental results.

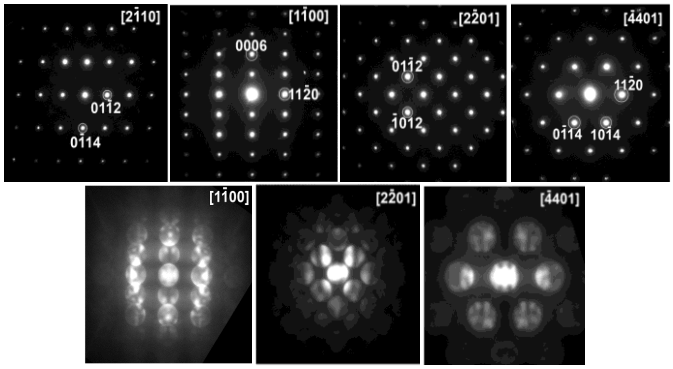

Figure 2. SAED (top panels) and CBED (bottom pannels) of Mn_2FeNbO_6 show the polar nature of the hexagonal cell.

Mn_2FeMO_6 (M = Nb, Ta) were prepared at 1573 K under 7 GPa in a Walker-type multianvil press (details of the synthesis are presented in Section 2 of the SI).[11] The powder synchrotron x-ray diffraction (SXRD) patterns of the as-prepared Mn_2FeMO_6 (Figure 1) could be indexed to rhombohedral unit cells (a ~5.27 Å, c ~ 13.9 Å), and Rietveld refinement quickly showed LN structure type. It is important to confirm the polar space group, therefore, convergent beam electron diffraction (CBED) and selected area electron diffraction (SAED) (Section 3 in SI) were used to determine the presence (*R-3c*) or absence (*R3c*) of an inversion center.[12] CBED patterns and tilt series of SAED patterns taken from Mn_2FeNbO_6 are shown on the bottom and top panels of Figure 2, respectively. These electron diffraction patterns could be completely indexed with the cell parameters from the XRD refinements. The reflection conditions derived from the patterns are: *hkil*: $-h + k + l = 3n$, *h-h0l*: $h + l = 3n$ and $l = 2n$ and *000l*: $l = 6n$. The 000*l*: $l = 6n + 3$ reflections that are observed on the [1$\bar{1}$00] are due to double diffraction, as is confirmed by the appearance of Gjonnes-Moodie lines through these reflections on the corresponding CBED pattern. Some of the [2$\bar{1}\bar{1}$0] zones show very weak sharp and some show weak diffuse reflections at 000*l*: $l = 6n + 3$ and $h\bar{h}0l$: $l = 2n + 1$, violating these reflection conditions. This can be due to the presence of local order. The trigonal extinction symbols matching these reflection conditions are R(obv)- - and R(obv) - *c*. The [*u-u.w*] zones [1$\bar{1}$00], [2$\bar{2}$01] and [4$\bar{4}$01] show as whole pattern symmetry *m*. Within the trigonal point groups, this whole pattern symmetry corresponds to point groups 32 and 3*m*. Combining the information from CBED and SAED leaves only the space group *R3c* as a possibility, in agreement with the SXRD results. Further observation of positive SHG effect also confirms the non-centrosymmetric character of the structure of both materials (Section 5 in SI).

Subsequent Rietveld refinements of the SXRD data are given in Section 4 of SI (Figure S3a, S3b; Table S1 and S2). The inset of Figure 1 shows a polyhedral view of the unit cell of Mn_2FeMO_6 (M = Nb, and Ta) with a typical LN-type structure, where Mn occupies a six coordinated A-site to form MnO_6 octahedra, and Fe and Nb are disordered on the six coordinated B-site in $(Fe/M)O_6$ octahedra. MnO_6 and $(Fe/M)O_6$ groups are arranged to avoid edge-sharing between homonuclear octahedra; the heteronuclear edge-shared octahedra, forming $[Mn(Fe/M)]O_{10}$ dimers, are arranged to form three-dimensional connectivity via face-sharing between the octahedral layers (Figure S1 of SI). The average <Mn-O> bond lengths are 2.16(1) and 2.22(2) Å for M = Nb and Ta, respectively and are comparable with the average <Mn-O> distance of MnO_6 octahedron in $Mn^{2+}Ti^{4+}O_3$ (2.199 Å)[13] and $Mn^{2+}{}_2Fe^{3+}Sb^{5+}O_6$ (2.173 Å)[9], but longer than those in $LaMn^{3+}O_3$ (2.020 Å)[16] and $YMn^{3+}O_3$ (2.036 Å)[14], which is consistent with the expected formal oxidation state of Mn^{+2} in Mn_2FeMO_6. As shown in Table S2, the Bond Valence Sum (BVS) for Mn (2.08+ and 1.94+ for M = Nb and Ta, respectively) agree well with the structural analysis results.[15] The metal-oxygen distances in the $(Fe/M)O_6$ ocahedra are 2.030(6) (M = Nb) and 2.012(20) Å (M = Ta), comparable to <Fe/M-O> of disordered B-sites perovskites, such as $Sr_2Fe^{3+}M^{5+}O_6$ (1.996 Å for M = Nb[16], 1.992 Å for M = Ta[17]), and $Pb_2Fe^{3+}M^{5+}O_6$ (2.005 Å for M = Nb[18] and Ta[19]). Thus, the crystal structure analysis indicates a cation formal oxidation state of $Mn^{2+}{}_2Fe^{3+}M^{5+}O_6$, which is further confirmed by x-ray absorption near edge spectroscopy (XANES) studies (Section 6 of SI).

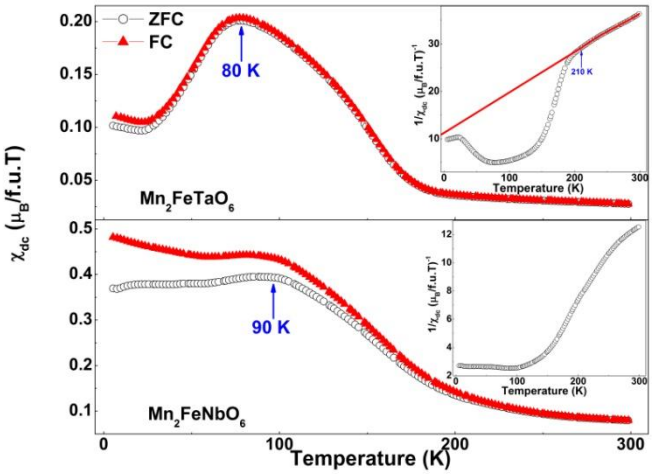

Figure 3. χ_{dc} *vs* temperature for Mn_2FeTaO_6 (top) and Mn_2FeNbO_6 (bottom) recorded in the ZFC as well as FC modes.The insets show the $1/\chi_{dc}$ *vs* T plots.

The magnetic properties of Mn_2FeMO_6 (M = Nb, Ta) show reproducible behavior on samples from different HP batches. Figure 3 shows the evolution of χ_{dc} *vs* temperature for Mn_2FeTaO_6 (top) and Mn_2FeNbO_6 (bottom) samples recorded in zero field cooled (ZFC) and field cooled (FC) modes. A clear difference in the behavior of the Nb and Ta samples is evident. For Mn_2FeTaO_6 (Figure 3 (top)), χ_{dc} shows a relatively sharp increase as the oxide is cooled below 200 K, indicating the emergence of magnetic order at this temperature. Below ~ 80 K, the magnetization starts falling rapidly. Note that this sharp drop is seen in both the ZFC and FC modes, thereby indicating a transition to a strong antiferromagnetic (AFM) state. The Mn_2FeNbO_6 sample, on the other hand, does not exhibit such sharp transitions (Figure 3 (bottom)). The emergence of magnetic order below 200 K is more gradual here. This is also clearly seen in the $1/\chi_{dc}$ vs T plots (insets of Figure 3), while the paramagnetic region above 200 K in Mn_2FeTaO_6 follows the Curie Weiss behavior (as evidenced by the linearity of the plot at T > 200

K), this is not the case for Mn_2FeNbO_6, where the $1/\chi_{dc}$ plot is not linear even for T > 200 K. In fact, the non-linearity extends well up to T = 300 K, which indicates the presence of residual magnetic interactions even at RT. Below ~ 90 K, there is a slight drop in the susceptibility of Mn_2FeNbO_6, both in the ZFC and FC curves, but in this case with a divergence between them, which indicate a transition to an AFM state with magnetic frustrations in the system. The high temperature inverse susceptibility data for the Mn_2FeTaO_6 sample could be fitted to a Curie-Weiss law, $\chi = C/(T-\theta_{CW})$. The fitting allowed us to extract the effective magnetic moment (μ_{eff}) = 10.07 μ_B, which agrees well with the calculated spin only moment per formula unit, μ_{calc} = 10.25 μ_B; for $\mu_{Mn2+} = \mu_{Fe3+}$ = 5.92 μ_B. The Curie-Weiss constant, obtained from the fitting, θ_{CW} = -165 K consistent with the presence of AFM interactions.

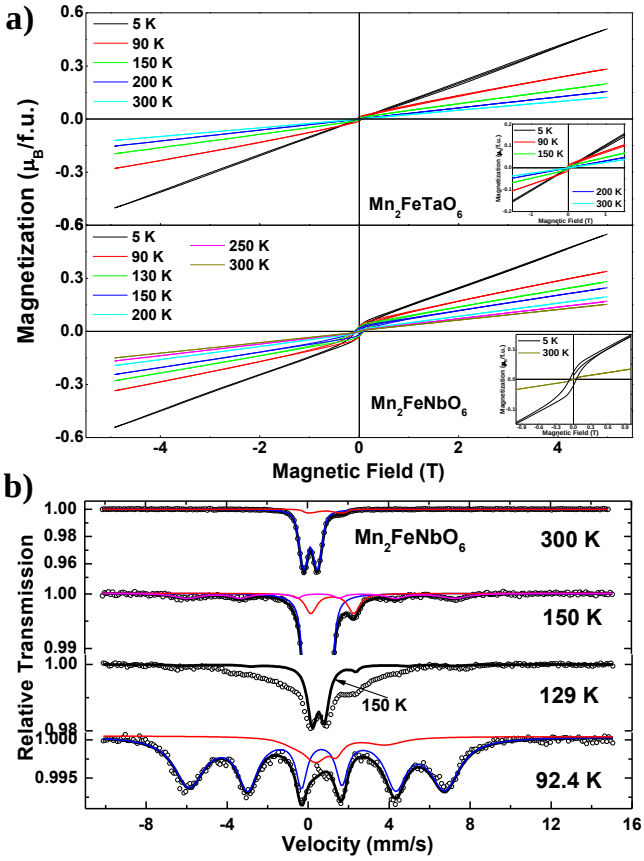

Figure 4. M *vs* H curves for (a) Mn_2FeTaO_6 (top) and Mn_2FeNbO_6 (bottom); (b) Mössbauer spectra of Mn_2FeNbO_6 between 90 and 300 K.

In Figure 4a (top), we show the isothermal M *vs* H curves of Mn_2FeTaO_6 recorded at various temperatures in the range 5 – 300 K. The inset of Figure 4a (top) shows an expanded view near the origin. For T > 200 K, the M *vs* H is perfectly linear with the curves passing through the origin. These curves correspond to the sample in the paramagnetic region. For T < 200 K, a small S-shaped hysteresis loop opens up near the origin. This is probably a manifestation of the emergence of canted ferromagnetism. It is important to note that the M-H curves show no sign of saturation for an applied magnetic field as high as H = 5 T indicating that the FM interactions are very weak, possibly due to spin canting. Below the AFM transition at T ~ 80 K, this S-shaped hysteresis loop vanishes, indicating a complete transition to the AFM state. The isothermal M-H curves of Mn_2FeNbO_6 (Figure 4a (bottom)) reveal a different behavior. The S-shaped hysteresis loop is present in this sample down to the lowest temperature measured (T = 5 K), which indicates that FM interactions, again possibly due to spin canting, are present even at low temperatures. Furthermore, even at the highest measured temperature (T = 300 K), the M-H curve is not perfectly linear (inset of Figure 4a (bottom)), thereby proving that the sample does not reach a pure paramagnetic state even at RT.

The magnetic nature of Mn_2FeMO_6 is further confirmed by Mössbauer spectra (Section 7 of SI). Figure 4b shows the Mössbauer spectra of Mn_2FeNbO_6, where the beginning of the appearance of the sextet at 150 K is observed, which suggests that the sample is at least partially ordered at this temperature. At 92 K the sextet is clearly resolved, consistent with a complete magnetic ordering. The data on Mn_2FeTaO_6 show similar behavior. Thus, we can conclude that the magnetic ordering temperatures in both samples are between 200 and 250 K. The Mössbauer study also provides information about the oxidation state and the positions occupied by Fe cations. The analysis of the data shows that ~92% of iron is trivalent, in good agreement with the XANES results. It also shows the existence of divalent iron (~8%), probably due to cation exchange between Mn and Fe in both A and B sites and/or oxygen defects, which cannot be distinguished by x-ray and electron diffraction studies, since the very similar x-ray scattering factors of Mn (Z = 25) and Fe (Z = 26) prevent unambiguous determination of the extent of ordering.

DFT+U calculations[20] (Section 8 of SI) indicate that both compounds have finite polarization due to the presence of d^0 ions Nb^{+5} and Ta^{5+}, while the magnetism arises due to presence of Mn and Fe. Figure 5 shows the exchange interaction between Mn and Fe to be of AFM nature. The magnetic lattice connecting Mn and Fe atoms consist of triangular arrangements which renders the AFM interaction frustrated. Such frustration may give rise to non-collinearity of spins. Our non collinear calculations gave rise to solution with canted magnetization axis of Mn and Fe spins and a small uncompensated net moment. The calculated noncollinear arrangement of spins may be checked by further experiments. The nominal d^5 valences of Mn and Fe, and d^0 valences of Nb and Ta have been confirmed also through spin polarized DFT+U calculations, which gave rise to calculated spin magnetic moments of about 4.2 – 4.5 μ_B at Mn and Fe sites, in conformity with high spin 2+ and 3+ valences of Mn and Fe, and a small moment of less than 0.05 μ_B at Nb or Ta site. The rest of the moment was found at O sites due to finite covalency effect.

The dielectric, dielectric pulse, and ferroelectric (FE) hysteresis measurements show that Mn_2FeMO_6 (M = Nb, Ta) are insulating paraelectrics at low temperature and paraelectric plus conducting at high temperature and room temperature (Figure S9 and S10 in Section 9 of SI). There is neither a FE P(E) hysteresis loop in ferroelectric measurements nor a sharp, divergence-like anomaly in the dielectric permittivity (ε') observed as expected for ferroelectric transitions. It is noteworthy that pyroelectricity was found in the samples at lower temperature, where the samples are not too conducting. Thus, the materials are polar

and pyroelectric but not ferroelectric, as the structural polarity is not switchable by external fields. Considering the symmetry with point group 3*m* (C3*v*), the polar axis is along the *c*-axis, the polarization, P, was estimated to be 32 and 23 $\mu C/cm^2$ for M = Nb, and Ta, respectively, from DFT calculations using the Berry phase formalism.[20a] Although DFT calculations are known to overestimate the value of polarization, this further indicates that Mn_2FeMO_6 are promising candidates for piezoelectric and pyroelectric as well as nonlinear optical materials.

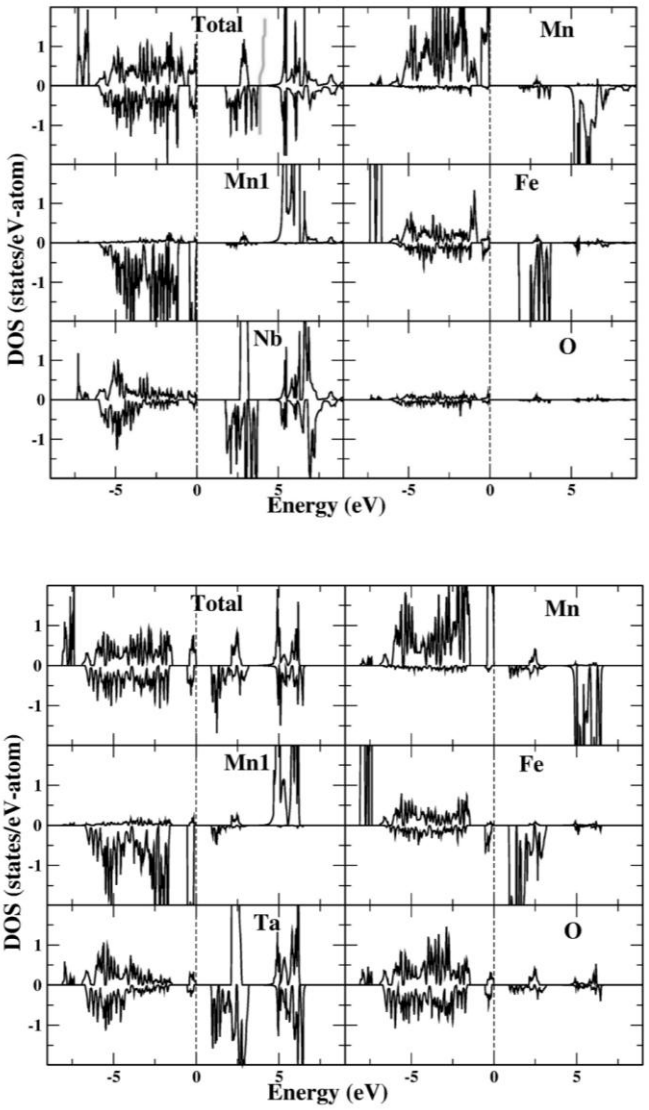

Figure 5. Total and Mn-*d*, Mn1-*d*, Fe-*d*, Nb/Ta-*d* and O-*p* projected density of states (DOS) for Mn_2FeNbO_6 (top panel) and Mn_2FeTaO_6 (bottom panel) compounds, as calculated in GGA+U approximation. The zero of the energy is fixed at the calculated Fermi energies

In conclusion, novel $LiNbO_3$-type polar magnetic oxides prepared by high pressure have been extended to the perovskite-related multiple B-sites $A_2BB'O_6$ system. The polar nature of the as-prepared $LiNbO_3$-type Mn_2FeMO_6 (M = Nb, Ta) is established by powder synchrotron x-ray and electron diffraction analyses, as well as by second harmonic generation effect, and theoretical calculations. These discoveries are of major significance and open up a new path for novel polar and magnetic materials. The variety of cations and structural versatility of the cation arrangement at both A and B sties in $A_2BB'O_6$, for example in the $A_2B^{3+}B'^{5+}O_6$ and $A_2B^{2+}B'^{6+}O_6$ series (A^{2+}), or $A_2B^{2+}B'^{4+}O_6$ (A^{3+}) could yield a large number of polar oxides, where A is an unusually small cation including Mg^{2+}, Mn^{2+}, Zn^{2+}, or Sc^{3+}, In^{3+}, and B' is a d^0 ion such as Nb^{5+}, Ta^{5+}, Mo^{6}, W^{+6}, or Ti^{4+}. These materials could be polar, and potentially multiferroic, piezoelectric, pyroelectric, and second-order nonlinear optical materials, with important technological applications.

Experimental Section

See Supporting Information. Further details of the crystal structure investigations may be obtained from the Fachinformationszentrum Karlsruhe, 76344 Eggenstein-Leopoldshafen, Germany, (fax: (49) 7247-808-666; e-mail :crysdata@fiz-karlsruhe.de) on quoting the deposition number CSD-425981 and -425982.

Received: ((will be filled in by the editorial staff))
Published online on ((will be filled in by the editorial staff))

Keywords: Density functional calculations · high pressure chemistry · $LiNbO_3$-type structure · Mn_2FeMO_6 · polar magnetic oxides

[1] K. M. Ok, E. O. Chi, P. S. Halasyamani, *Chem. Soc. Rev.* **2006**, *35*, 710-717.
[2] M. D. Donakowski, R. Gautier, J. Yeon, D. T. Moore, J. C. Nino, P. S. Halasyamani, K.. R. Poeppelmeier, *J. Am. Chem. Soc.* **2012**, *134*, 7679-7689.
[3] a) A. A. Belik, T. Furubayashi, H. Yusa, E. Takayama-Muromachi, *J. Am. Chem. Soc.* **2011**, *133*, 9405-9412; b) M. R. Li *et al.*, see Supporting Information, *J. Am. Chem. Soc.* **2012**, *134*, 3737-3747.
[4] a) Y. Inaguma, M. Yoshida, T. Katsumata, *J. Am. Chem. Soc.* **2008**, *130*, 6704-6705; b) I. Yoshiyuki, Y. Masashi, T. Takeshi, A. Akihisa, T. Kie, K. Tetsuhiro, M. Daisuke, *J. Phys.: Conf. Ser.* **2010**, *215*, 01231.
[5] A. A. Belik, T. Furubayashi, Y. Matsushita, M. Tanaka, S. Hishita, E. Takayama-Muromachi, *Angew. Chem.* **2009**, *121*, 6233-6236; *Angew. Chem. Int. Ed.* **2009**, **48**, 6117-6120.
[6] A. Aimi, T. Katsumata, D. Mori, D. FU, M. Itoh, T. Kyômen, K. Hiraki, T. Takahashi, Y. Inaguma, *Inorg. Chem.* **2011**, *50*, 6392-6398.
[7] T. Varga *et al.*, see Supporting Information, *Phys. Rev. Lett.* **2009**, *130*, 047601.
[8] K. I. Kobayashi, T. Kimura, H. Sawada,K. Terakura, Y. Tokura, *Nature*, **1998**, *395*, 677-680.
[9] G. V. Bazuev, B. G. Golovkin, N. V. Lukin, N. I. Kadyrova, Y. G. Zainulin, *J. Solid State Chem.* **1996**, *124*, 333-337.
[10] R. Mathieu, S. A. Ivanov, I. V. Solovyev, G. V. Bazuev, P. Anil Kumar, P. Lazor, P. Nordblad, *Phys. Rev. B* **2013**, *87*, 014408.
[11] D. Walker, M. A. Carpenter, C. M. Hitch, *Am. Mineral.* **1990**, *75*, 1020-1028.
[12] J. C. H. Z. Spencce, J. M. Zuo, *Electron Microdiffraction*. Plenum Press: New York, **1992**.
[13] J. Ko, C. Prewitt, *Phys. Chem. Miner.* **1988**, *15*, 355-362.
[14] N. Lliev, M. V. Abrashev, H. G. Lee, V. N. Popov, Y. Y. Sun, C. Thomsen, R. L. Meng, C. W. Chu, *J. Phys. Chem. Solids*, **1998**, *59*, 1982-1984.
[15] N. E. Brese, M. O'Keeffe, *Acta Crystallogr. B*, **1991**, *47*, 192-197.
[16] W. L. Michael, B. M. Ren é, L. Yongjae, V. Thomas, L. Hans-Conrad zur, *J. Phys.: Condens. Matter.* **2006**, *18*, 8761…
[17] E. J. Cussen, J. Vente, P. D. Battle, T. C. Gibb, *J. Mater. Chem.* **1997**, *7*, 459-463.
[18] L. Nathascia, S. Philippe, L. Alessandra Geddo, *J. Phys.: Condens. Matter* **1999**, *11*, 3489.
[19] L. Nathascia, S. Philippe, L. Alessandra Geddo, *J. Phys.: Condens. Matter* **2000**, *12*, 2367.
[20] a) J. P. Perdew, K. Burke, M. Ernzerhof, *Phys. Rev. Lett.* **1996**, *77*, 3865. b) V. I. Anisimov, J. Zaanen, O. K. Andersen, *Phys. Rev. B* **1991**, *44*, 943. c) G. Kresse, J. Hafner, *Phys. Rev. B* **1993**, *47*, 558. d) G. Kresse, D. Houbert, *Phys. Rev. B* **1999**, *59*, 1758.

Entry for the Table of Contents (Please choose one layout)

Polar Magnetic Oxides

Man-Rong Li, David Walker, Maria Retuerto, Tapati Sarkar, Christoph P. Grams, Joke Hardermann, Peter W. Stephens, Mark Croft, Alexander Ignatov, Joachim Hemberger, Israel Nowik, P. Shiv Halasyamani, T. Thao Tran, Swarnakamal Mukherjee, Tanusri Saha Dasgupta, Martha Greenblatt*

_____ **Page – Page**

Polar and Magnetic Mn_2FeMO_6 (M = Nb, Ta) with $LiNbO_3$-type Structure - High Pressure Synthesis

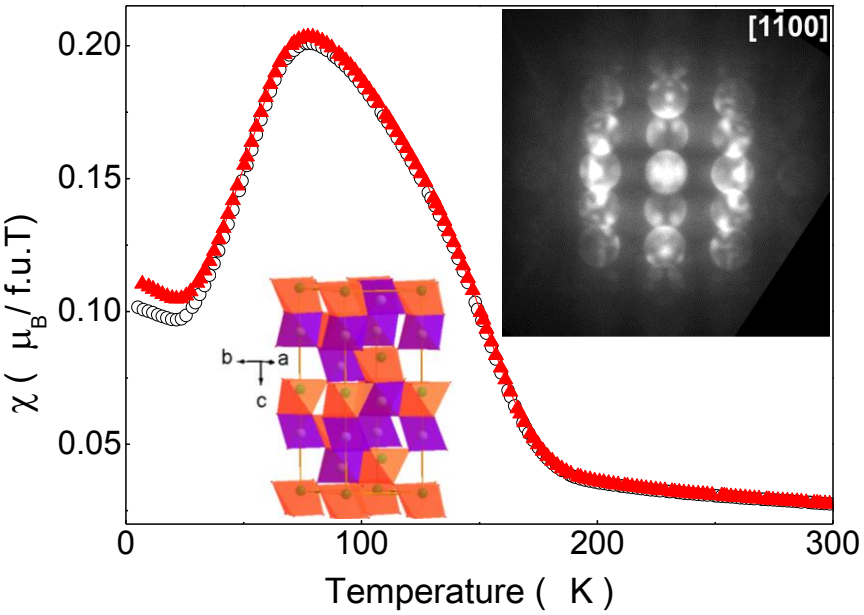

Polar $LiNbO_3$-type magnetic oxides have been extended, for the first time, to the $A_2BB'O_6$ family. The high pressure synthesized $Mn^{2+}{}_2Fe^{3+}M^{5+}O_6$ (M = Nb, Ta) adopt a polar structure as demonstrated by electron diffraction and second harmonic generation effect and they present interesting magnetic properties. These experimental findings as well as theoretical calculations surely open a new area in the search for novel multifunctional polar materials.

Supporting Information

Full information of Reference [3b] and [7]:

[3] b) M. R. Li, A. Umut, S. R. C. McMitchell, Z. Xu, C. I. Thomas, J. E. Warren, D. V. Giap, H. Niu, X. Wan, R. G. Palgrave, F. Schiffmann, F. Cora, B. Slater, T. L. Burnett, M. G. Cain, A. M. Abakumov, G. Tendeloo van, M. F. Thomas, M. J. Rosseinsky & J. B. Claridge J. *Am. Chem. Soc.* **2012**, *134*, 3737-3747.

[7] T. Varga, A. Kumar, E. Vlahos, S. Denev, M. Park, S. Hong,T. Sanehira, Y. Wang, C. J. Fennie, S. K. Streiffer,X. Ke, P. Schiffer, V. Gopalan, & J. F. Mitchell, *Phys. Rev. Lett.* **2009**, *103*, 047601.

Polar and Magnetic Mn_2FeMO_6 (M = Nb, Ta) with $LiNbO_3$-type Structure-High Pressure Synthesis

Man-Rong Li[a], David Walker[b], Maria Retuerto[a], Tapati Sarkar[a], Joke Hadermann[c], Peter W. Stephens[d], Mark C. Croft[e], Alexander Ignatov[e], Christoph P. Grams[f], Joachim Hemberger[f], Israel Nowik[g], P. Shiv Halasyamani[h], T. Thao Trang[h], Swarnakamal Mukherjee[i] Tanusri Saha Dasgupta[i], Martha Greenblatt[a]*

[a] *Department of Chemistry and Chemical Biology, Rutgers, The State University of New Jersey,610 Taylor Road, Piscataway, NJ 08854, USA*

[b] *Lamont-Doherty Earth Observatory, Columbia University,61 Route 9W-PO Box 1000, Palisades, NY 10964, USA*

[c] *EMAT, University of Antwerp, Groenenborgerlaan 171, B-2020 Antwerp, Belgium*

[d] *Department of Physics & Astronomy, State University of New York, Stony Brook, NY 11794, USA*

[e] *Department of Physics and Astronomy Rutgers, The State University of New Jersey,136 Frelinghuysen Road, Piscataway, NJ 08854, USA*

[f] *II. Physikalisches Institut, Universität zu Köln,D-50937 Köln, Germany*

[g] *Racah Institute of Physics Hebrew University, Jerusalem, 91904, Israel*

[h] *Department of Chemistry, University of Houston,136 Fleming Building, Houston, TX 77204, USA*

[i] *Department of Condensed Matter Physics and Materials Sciences, S. N. Bose National Centre for Basic Sciences, JD Block, Sector III, Salt Late, Kolkata 700098, India*

Email: martha@rutchem. rutgers.edu

1. Comparison of corundum, ilmenite (IL) and $LiNbO_3$ (LN) type crystal structures

Generally, exotic ABO_3 perovskites with unusually small A-site cations can form corundum, IL, or LN type structure under high pressure.[1-3] The crystal structures of corundum, IL, and LN materials are show in Fig. S1. In these structures both the A and B cations are six coordinated with oxygen forming octahedra. The structure is formed by layers of edge-sharing octahedral dimers (highlighted by dashed green lines, Fig. S1), which are linked between the layers via face-sharing (highlighted by black dashed lines, Fig. S1), to build a three-dimensional network structure. In the corundum structure the A- and B cations are disordered and the space group, *R3c* is centrosymmetric (CS). In both the IL (CS space group *R-3*) and LN (non-centrosymmetric (NCS) space group *R3c*) the A- and B-site cations order, but the edge-sharing octahedral layers are arranged differently. In the IL structure, the layers are formed by homonuclear edge-sharing AO_6 or BO_6 octahedra (Fig. S1b), while in the LN structure, the AO_6 and BO_6 octahedra are arranged to avoid edge-sharing between the same kind of octahedra in the layers (Fig. S1c).

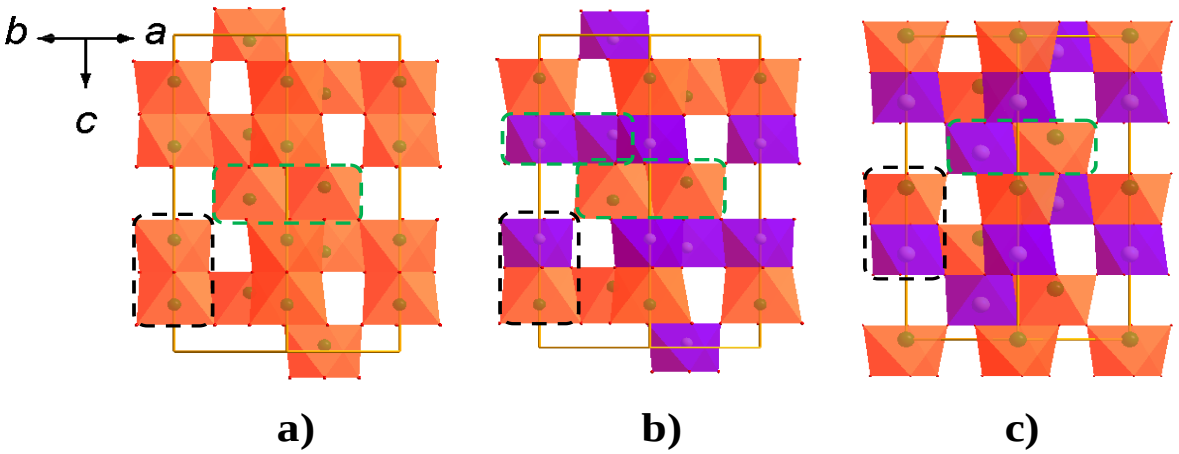

Fig. S1 The crystal structures of (a) corundum, (b) IL and (c) LN view along [110] direction. The edge-sharing octahedral dimers in layers are highlighted by green dashed lines and the face-sharing octahedral dimers by black dashed lines,. In (b) and (c), AO_6 octahedra are orange and BO_6 octahedra are blue.

2. Ambient pressure (AP) and high pressure (HP) syntheses of Mn_2FeMO_6 (M = Nb, Ta)

Attempts to prepare Mn_2FeMO_6 (M = Nb, Ta) at AP were unsuccessful. Stoichiometric mixtures of MnO (99.99%, Alfa Aesar), Fe_2O_3 (99.999%, Sigma Aldrich), and Nb_2O_5 (Alfa Aesar, 99.9985%) or Ta_2O_5 (99.85%, Alfa Aesar) were pressed to form a pellet and annealed at 1250 -1300 ^oC for 12 h under Ar atmosphere, but mainly yielded $Mn_4M_2O_9$ (M = Nb, Ta)[4] and the spinel phase $MnFe_2O_4$[5], as shown in the lab x-ray diffraction (XRD) patterns (Fig. S2) collected on a Bruker D8-Advance Diffractometer with a SOL-X solid state detector.

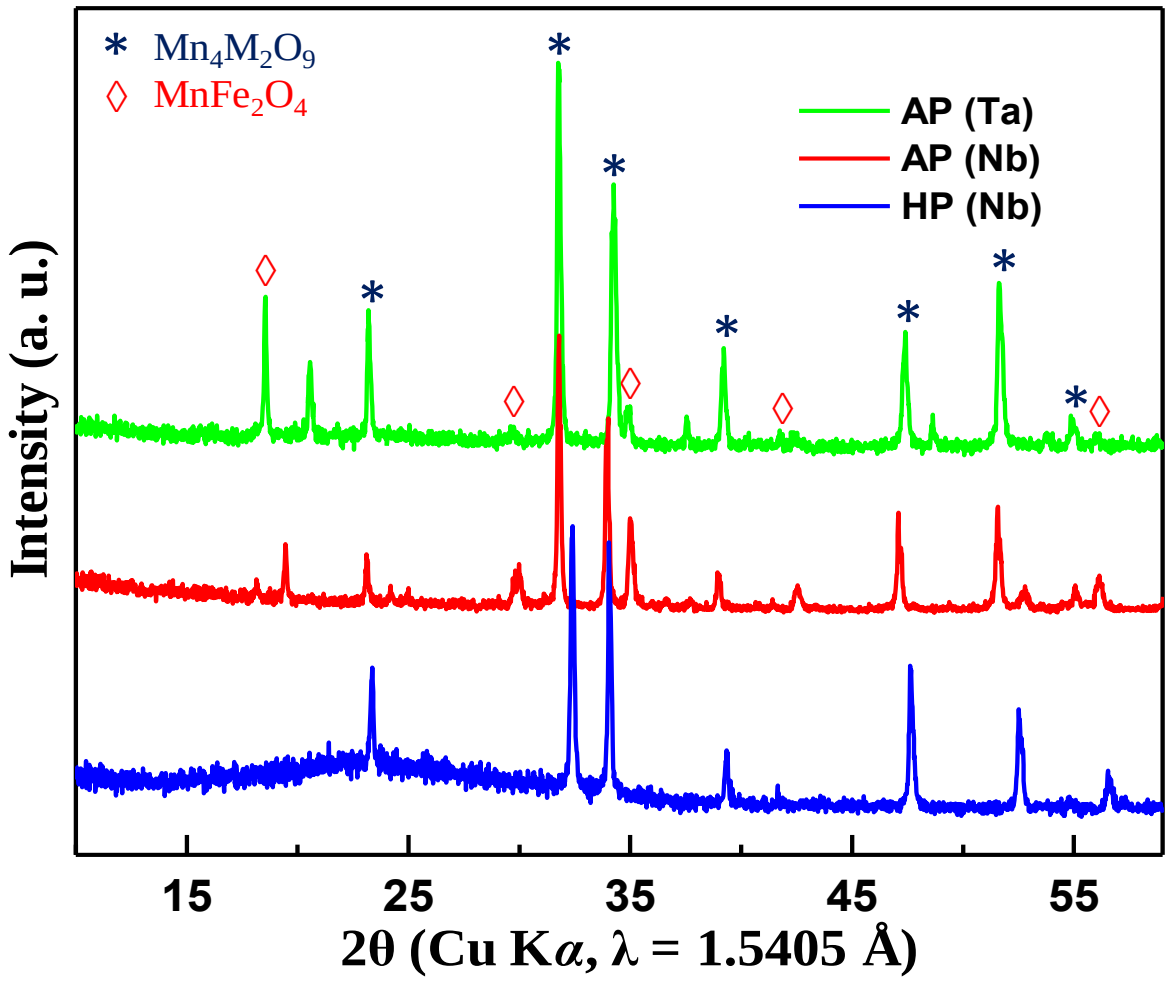

Fig. S2 Room temperature XRD patterns of Mn_2FeMO_6 (M = Nb, Ta) prepared under AP, resulting in $Mn_4M_2O_9$ and $MnFe_2O_4$ spinel phases. The XRD patterns of high pressure $LiNbO_3$-type Mn_2FeNbO_6 was also added for comparison.

The small Mn^{2+} cation at the A-site gives tolerance factors of 0.869 and 0.867 for M = Nb and Ta, respectively, assuming the most favorable formal oxidation state of Mn^{2+} (high spin, HS), Fe^{3+} (HS), and Nb^{5+}/Ta^{5+} (d^0).[6,7] These small tolerance factors predict unstable perovskite-related $A_2BB'O_6$ compounds under ambient pressure conditions. The target Mn_2FeMO_6 (M = Nb, Ta) were prepared from stoichiometric mixtures of the above starting materials. The oxide mixture was reacted at 1573 K under 7 GPa for 0.5-1 h in a $LaCrO_3$ heater lined with Pt capsule inside a MgO crucible in a Walker-type Multianvil press, and then quenched to room temperature by turning off the voltage supply to the resistance furnace, which reduced the temperature to room temperature in a few seconds. The pressure is maintained during the temperature quenching and then decompressed slowly.

3. **Electron diffraction**

Samples for electron microscopy were prepared by dispersing the powder in ethanol and depositing on a holey carbon grid. Selected area electron diffraction (SAED) and convergent beam electron diffraction (CBED) patterns were obtained on a Philips CM20 transmission electron microscope. High resolution transmission electron microscopy (HR-TEM) patterns were obtained with a Tecnai G2 transmission electron microscope.

4. **Powder x-ray synchrotron diffraction (SXRD) refinements**

Powder SXRD data were recorded on beam line X-16C (λ = 0.6997 Å) at the Brookhaven National Synchrotron Light Source (NSLS). Diffraction data analysis and Rietveld refinement was performed with the TOPAS software package.[8] The polar $LiNbO_3$-type model (*R3c*) gave

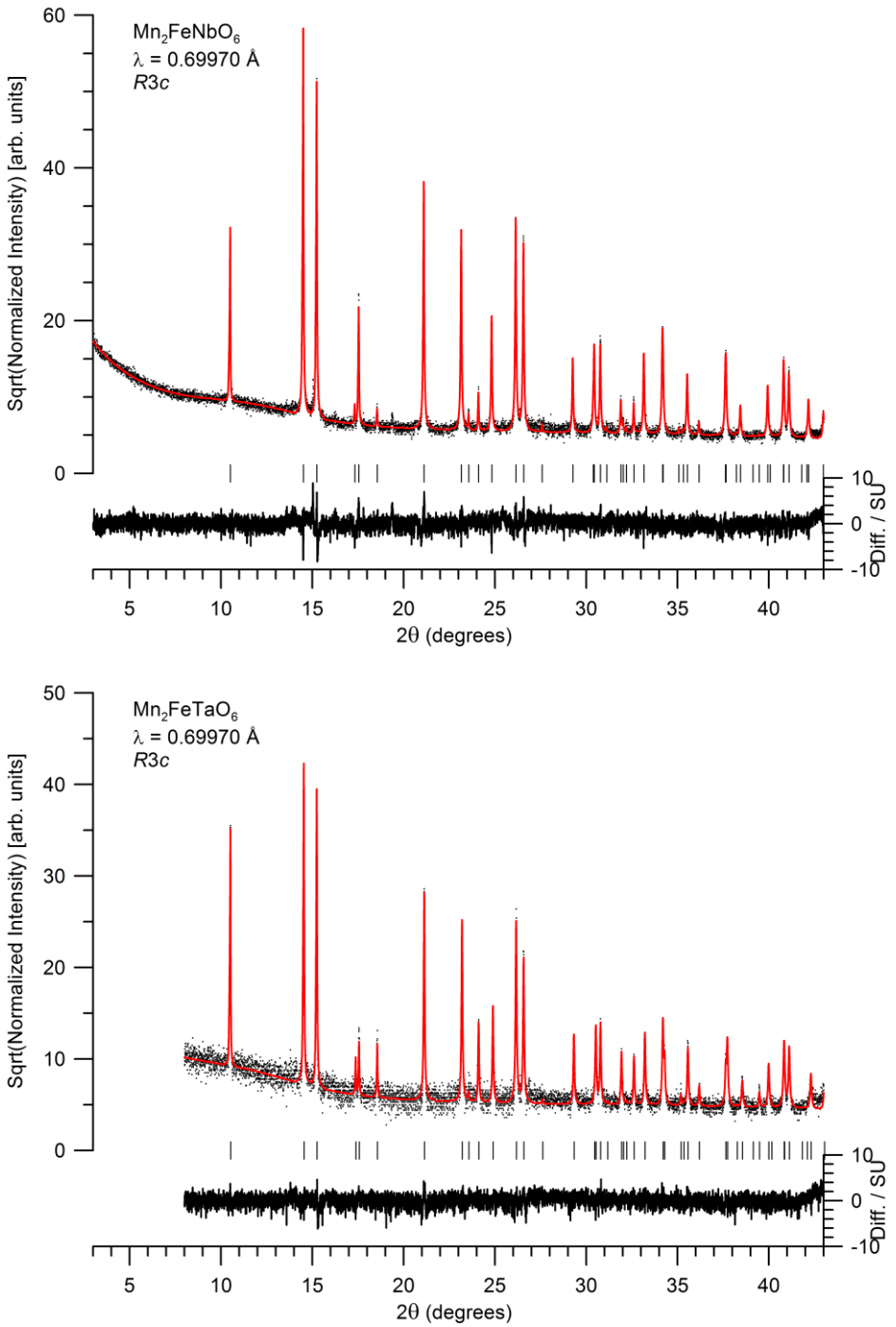

Fig. S3 Experimental, calculated, and difference powder SXRD patterns of Mn_2FeNbO_6 (top) and Mn_2FeTaO_6 (bottom) after Rietveld refinements in $LiNbO_3$-type structural model. The vertical bars below the diffraction patterns are the expected reflection positions.

excellent agreement between the observed and calculated SXRD patterns for both Mn_2FeNbO_6 and Mn_2FeTaO_6 as shown in Fig. S3 and Table S1, S2. In the octahedral dimers, Mn and Fe/M are displaced away from the octahedral centroids in opposite directions towards one of the octahedral faces (local C_3 direction), as also found in other LN-type compounds. This displacement results in three long and three short metal-oxygen bonds in both MnO_6 and $(Fe/M)O_6$ octahedra (Fig. S4 and Table S2).

Table S1 Structural parameters, R factors, and bond valence sums (BVS) of Mn_2FeMO_6 (M = Nb, Ta) refined in polar LN-type structure .

Mn_2FeMO_6	**M = Nb**	**M = Ta**
Space group	*R3c*	*R3c*
a/Å	5.2740(1)	5.2721(1)
c/ Å	13.9338(2)	13.8892(3)
V/ Å^3	335.65(1)	334.33(1)
Mn		
Wyck.	6*a*	6*a*
B/ Å^2	0.42(2)	0.07(3)
Occupancy	1	1
Fe/M		
Wyck.	6*a*	6*a*
z	0.219(1)	0.2175(3)
B/ Å^2	0.42(2)	0.07(3)
Occupancy	0.5/0.5	0.5/0.5
O		
Wyck.	18*b*	18*b*
x	0.315(3)	0.305(5)
y	0.034(2)	0.043(3)
z	0.120(1)	0.1227(17)
B/ Å^2	0.42(2)	0.07(3)
Occupancy	1	1
R_p, R_{wp}, R_{exp}	0.078, 0.104, 0.080	0.146, 0.192, 0.157

Table S2 Selected bond lengths and bond angles of Mn_2FeMO_6 (M = Nb, Ta) refined in polar LN-type structure

Mn_2FeMO_6	**M = Nb**	**M = Ta**
	Selected bond lengths/Å	
MnO_6		
Mn-O ×3	2.01(1)	2.14(2)
-O ×3	2.30(1)	2.29(2)
<Mn-O>	2.155	2.215
BVS	2.08	1.94
$(Fe/M)O_6$		
(Fe/M)-O ×3	1.97(1)	2.00(2)
-O ×3	2.10(1)	2.02(2)
<Fe/M-O>	2.035	2.01
BVS	2.89/4.35	3.05/4.71
	Selected bond angles/°	
Mn-O-Mn	121.3(5)	119.4(7)
Mn-O-Fe/M	87.8(4)	88.9(8)
	93.9(5)	93.2(9)
	96.8(5)	97.4(9)
	115.4(6)	112.4(10)
Fe/M-O-Fe/M	140.4(5)	144.1(8)
O-Mn-O	73.0(4)	70.7(7)
	79.8(5)	78.3(8)

	88.9(5)	89.9(8)
	110.8(5)	112.2(8)
	150.8(5)	147.4(8)
O-Fe/M-O	81.4(5)	82.0(9)
	87.8(6)	88.3(9)
	90.4(5)	91.5(8)
	99.0(6)	97.2(9)
	167.3(5)	168.9(9)

It is important to comment on the differences found in the structures of Mn_2FeMO_6 (M = Nb, Ta) compared to Mn_2FeSbO_6.[9] Although the ionic radii of six coordinated Sb^{5+} (0.60 Å), Nb^{5+} (0.64 Å), and Ta^{5+} (0.64 Å) are very similar,[5] Mn_2FeSbO_6 crystallizes in a CS IL structure

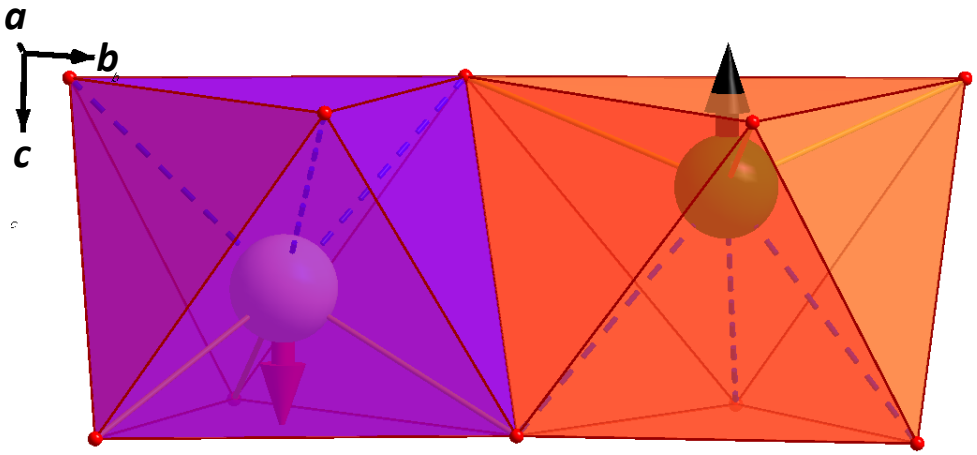

Fig. S4 Edge-sharing octahedral $Mn(Fe/M)O_{10}$ dimer in the crystal structure of Mn_2FeMO_6 (M = Nb, Ta), where Mn and Fe/M displace away from the central position of each octahedron (MnO_6, orange; $(Fe/M)O_6$, blue) towards one of the octahedral faces in opposite direction, resulting in three short and three long metal-oxygen bond lengths. The three long metal-oxygen bonds are highlighted by dashed lines. The arrows show the metal displacement directions.

while Mn_2FeMO_6 (M = Nb, Ta) in a non-CS polar LN-type structure with all of the cations with 6-fold oxygen coordination: Nb^{5+} and Ta^{5+} at the B-site and Mn^{2+} (0.83 Å, HS) at the A-site. The reason for the difference between the structures could be related to the difference of electronic configuration between Sb^{5+} (d^{10}) and Nb^{5+} and Ta^{5+} (d^0).[5] In these octahedrally coordinated d^0 transition metal oxides the spin polarization is energetically favorable for the formation of the polar LN-type instead of the IL structure as shown in the DFT calculation in Section 8.

5. **Second-harmonic generation (SHG) measurements**

Powder SHG measurements at room temperature were performed on a modified Kurtz nonlinear optical system with a pulsed Nd : YAG laser of wavelength 1064 nm.[10] Known SHG crystalline SiO_2 (quartz) powder was also applied to make relevant comparisons. All of the powders were placed in separate capillary tubes. The SHG, i.e., 532 nm green light, radiation was collected in reflection mode and detected by a photomultiplier tube (Oriel Instruments). To detect only the SHG light, a 532 nm narrow-band-pass interference filter was attached to the tube. A digital oscilloscope (Tektronix TDS 3032) was used to monitor and collect the SHG signal.

The SHG intensity of both Mn_2FeNbO_6 and Mn_2FeTaO_6 are comparable to that of the SHG active α-SiO_2 as green light (532 nm, half of that of the radiation of 1064 nm). Since the corresponding point group 3*m* (*C*3V) belongs to a polar crystal class, detection of the SHG signal is consistent with the structural symmetry from electron diffraction analyses.

6. X-ray absorption near edge spectroscopy (XANES)

X-ray absorption near edge spectroscopy (XANES) was carried out to further confirm the formal oxidation state of the cations in Mn_2FeMO_6. Mn, Fe and Ta XANES were collected on the beam line X-19A at Brookhaven NSLS in both transmission and fluorescence modes with simultaneous standards. Nb XANES was collected in fluorescence mode in a He-atmosphere-

chamber with standards run. The main edge features at 3-*d* transition metal K edges are dominated by 1*s* to 4*p* transitions. These features, and the step-feature continuum onset which lies underneath them, manifest a chemical shift to higher energy with increasing valence. The 4*p* features can also be split into multiple features by the local atomic coordination/bonding and by final state effects (i.e. admixed 3*d* configurations). The chemical shift of the K edge has been widely used to chronicle the evolution of the transition metal valence state in oxide-based materials.[11-15] In Fig. S5 and S6 the Mn- and Fe-K edges for the Mn_2FeMO_6 (M = Nb and Ta) compounds are compared to a series of standard compounds. The nominal proximity of the main edge rise for various formal valence states is indicated by a square in the figures. It is worth

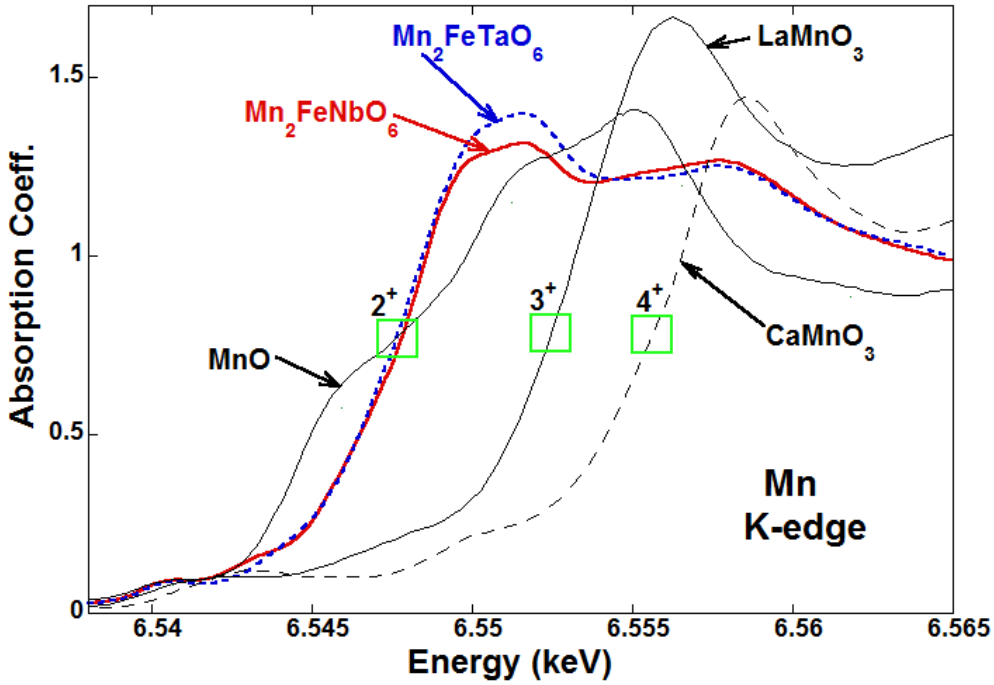

Fig. S5 The Mn-K edge spectra for the Mn_2FeMO_6 (M = Nb and Ta) series of octahedral O-coordinated Mn compounds with varying formal valences: $Mn^{2+}O$, $LaMn^{3+}O_3$, and $CaMn^{4+}O_3$. Here, and subsequently, the formal valence is used ignoring more subtle hybridization/covalency effects.

noting that the MnO and FeO standards (with edge sharing Mn/Fe-O octahedra) manifest a robust two feature rise and the chemical shift is identified (here) roughly with the inflection point between the two. The less structured steeply rising Mn-K edges of the Mn_2FeMO_6 compounds exhibit a chemical shift consistent with MnO, which is the Mn^{2+} standard and are clearly much lower in energy than the Mn^{3+} and Mn^{4+} standards. Thus the formal oxidation state at the Mn sites in these compounds is consistent with Mn^{2+}. In Fig. S6, the chemical shift for the Fe-K edges for Mn_2FeMO_6 (M = Nb and Ta) falls in the formal Fe^{3+} valence range.

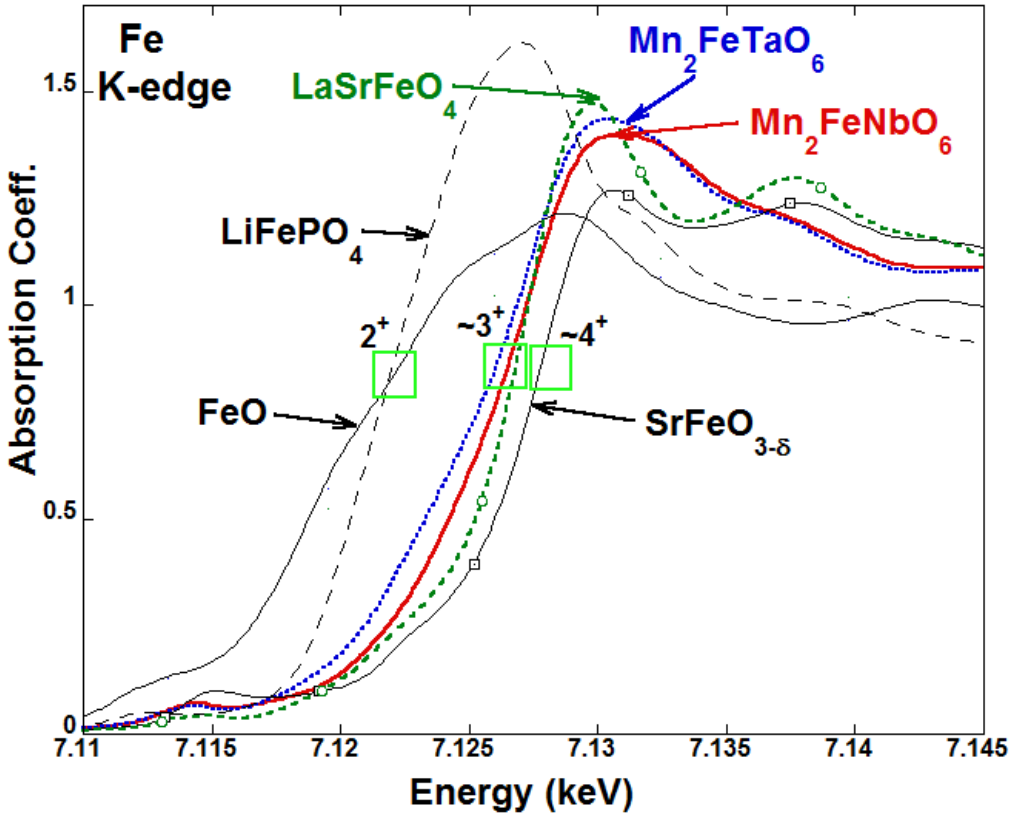

Fig. S6 The Fe-K edge spectra for the Mn_2FeMO_6 (M = Nb and Ta) compounds along with a series of octahedral O-coordinated Fe compounds with varying formal valences: $Fe^{2+}O$, $LiFe^{2+}PO_4$,$LaSrFe^{\sim 3+}O_4$, and $SrFe^{\sim 4+}O_3$.

Fig. S7 and S8 show the Nb and Ta L_3-edges for Mn_2FeNbO_6 and Mn_2FeTaO_6, respectively, together with the corresponding standards. The intense peak features at the L_3-edges of 4*d*/5*d* transition metals (T) involve 2*p*-core to 4*d*/5*d* final-state transitions.[15-21] These features can provide a probe of the empty 4*d* state energy distribution, albeit modified by the transition matrix element, core–hole interaction and multiplet effects.[15-21] In the octahedral coordination, typical of perovskite based compounds, the transition metal *d*-states are split into

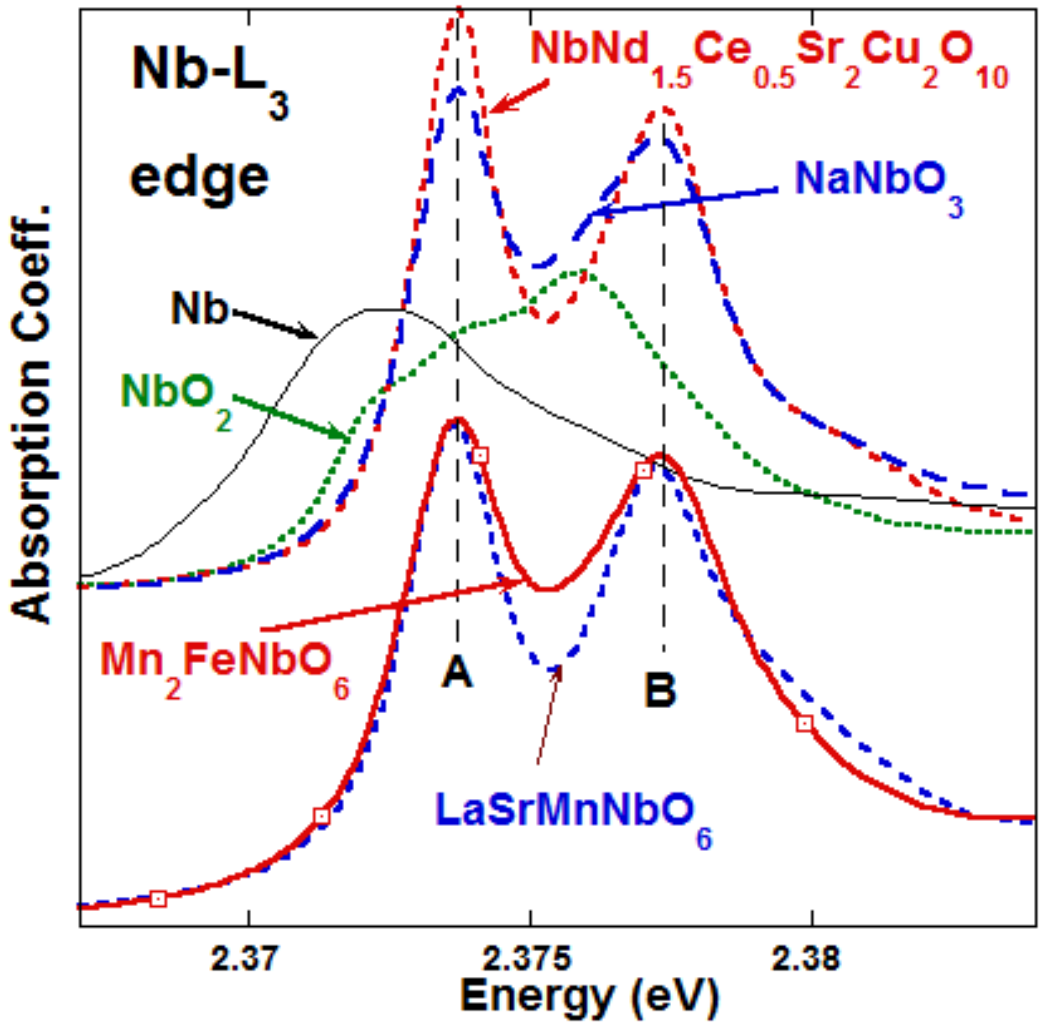

Fig. S7 The Nb-L_3 edge of Mn_2FeNbO_6 overlayed (for reference) with that of $LaSrMnNbO_6$ (bottom of figure). A comparison (top) of the Nb-L_3 standard spectra for: $NaNbO_3$ and $NbNd_{1.5}Nd_{0.5}Sr_2Cu_2O_{10}$ (both Nb^{5+}~4d^0), NbO_2 (Nb^{4+}~4d^1) and elemental Nb.

lower energy, t_{2g} (sextet) and a higher energy e_g (quartet) states. In low-*d*-occupancy transition metals (as Nb and Ta), the T L_3-edges display a robust two peak structure with the lower energy peak (A) involving transitions into empty t_{2g} states; and the high-energy peak (B) involving excitations into empty e_g states (Fig. S7 and S8). Thus for *d*-hole counts greater than 4 the B-feature intensity reflects the empty e_g states and the intensity of the A-feature scales with the number of t_{2g}-holes. Thus the A-feature intensity, relative to that of the B-feature, provides an indicator of the T 5*d* count/valence state. This effect is well illustrated in the left side of Fig. S8 where a comparison of the T L_3-edges of ~$5d^0$ and ~$5d^1$ compounds has been made. In the ~$5d^0$ compounds (W^{6+} and Ta^{5+}), the peak intensity of the A-feature is more intense, and in the ~$5d^1$

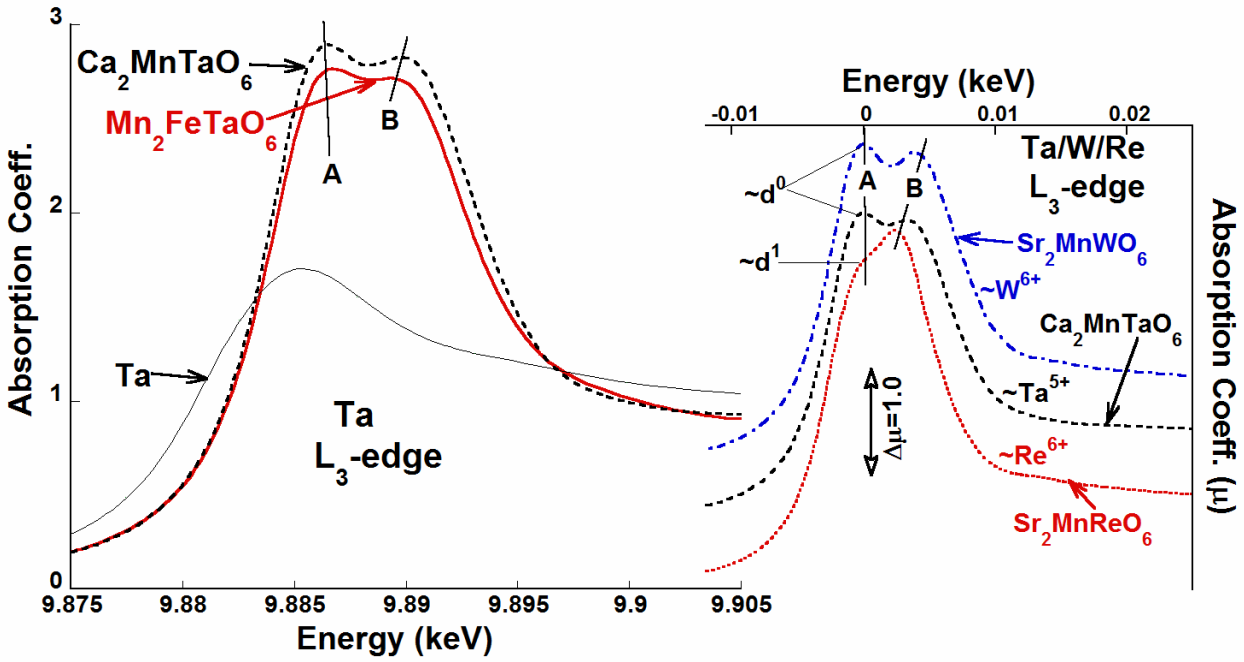

Fig. S8 (a) The Ta-L_3 edge spectra for Mn_2FeTaO_6 compared to $Ca_2FeTa^{5+}O_6$ and elemental-Ta standards; (b) Comparison of the T-L_3 edge spectra (T= Ta, W, Re) for the ~$5d^0$ compounds $Ca_2FeTa^{5+}O_6$ and $Sr_2MnW^{6+}O_6$ compared to the ~$5d^1$ compound $Sr_2MnRe^{6+}O_6$.

compound (Re^{6+}), it is less intense than the B-feature. In Fig. S8, (Ta L_3-edges of Mn_2FeTaO_6) the Ta^{5+} standard Ca_2FeTaO_6 and elemental Ta (for reference) are shown. The relative A-feature intensity for the Mn_2FeTaO_6 spectrum clearly indicates a Ta^{5+} (~d^0) configuration in this compound.

The bimodal A-B peak structure at the L_3-edge of octahedrally coordinated 4*d* row compounds is similar to the 5*d* example above, but with better resolution due to the narrower 4*d* bands, the smaller core hole lifetime broadening and the better instrumental resolution at the much lower energy. The signature of Nb^{5+}-d^0 *vs*. Nb^{4+}-d^1 configuration is that the A-feature intensity is larger than the B-feature intensity in the former (as has been explained above) [22]. This has been well-illustrated in Mo^{6+}-d^0/Mo^{5+}-d^1 compounds studied by our group in the past. In Fig. S7, the relative A-feature intensity of the Mn_2FeNbO_6 spectrum clearly indicates formally Nb^{5+}-d^0 state. A further confirmation of this configuration is the chemical shift of the Mn_2FeNbO_6 spectrum to higher energy relative to the $Nb^{4+}O_2$ standard, as expected for the Nb^{5+}-d^0 state. Clearly, the XANES results indicate the formal oxidation state of $Mn^{+2}{}_2Fe^{+3}M^{+5}O_6$, and further support the atomic environment and electron configurations suggested by the crystal structure analysis.

7. Mössbauer spectroscopy and magnetism measurements

Mössbauer data were obtained with a conventional constant acceleration Mössbauer spectrometer incorporating a ~50 mCi source of Co^{57} in a Rh matrix. The absorbers were cooled in a closed-cycle refrigerator (Janis, Model SHI-850-5). Magnetization measurements were carried out with a commercial Quantum Design superconducting quantum interference device (SQUID) magnetometer. The susceptibility was measured in zero field cooled (ZFC) and field

cooled (FC) conditions under a 0.1 T magnetic field, for temperatures ranging from T = 5 to 300 K. Isothermal magnetization curves were obtained at T = 5-300 K under an applied magnetic field that varied from -5 to 5 T.

8. DFT calculation

The calculations have been performed within the generalized gradient approximation (GGA)[23] of the exchange-correlation functional with the choice of Perdew-Burke-Ernzerhof (PBE) functional[24] in a spin polarized scheme. To improve the description of correlation effects in Mn and Fe-d electrons, a DFT+U[25-27] method within the Dudarev et al.'s approach is used. We have chosen a U_{eff} = (U -J) value of 4.2 eV at the Mn and Fe sites which has been shown to provide good results. The effect of variation of U_{eff} on calculated properties is found to be minimal. The calculations were performed in plane wave basis as implemented in Vienna Ab-initio Simulation Package (VASP).[28-30] For these plane wave calculations, we used projector augmented wave (PAW) potentials[31] and the wave functions were expanded in the plane wave basis with a kinetic energy cutoff of 600 eV. Reciprocal space integrations were carried out with a k mesh of 5 x 5 x 5. The crystal structures were optimized starting from the experimentally measured structures, fixing the lattice constants at experimentally determined values, until the total forces on each ion were converged to better than 0.01 eV/A^o. For the density of states calculations, a Gaussian smearing of 0.1 eV was used. We calculate the electronic contribution to the polarization as a berry phase using the method developed by King-Smith and Vanderbilt[32], and extract the ionic contribution by summing the product of the position of each ion with its pseudo-charge.

9. Dielectric and ferroelectric property measurements

The dielectric properties were measured using a NovoControl-Alpha frequency response analyzer. The ferroelectric P-E loops were recorded with a modified Sawyer-tower circuit employing a Keithley 6517 electrometer. The samples were sandwiched between Ag paste deposited electrodes, in parallel plate geometry for the above measurements.

As shown in Fig. S9 and S10, the measurements of the dielectric properties indicates that the dispersive high values at high temperature are again due to electrodes (contacts) or sample heterogeneities (grain boundaries) and (hopping) conductivity (compare e.g. [33]). The intrinsic ε' one can see at low temperature where the different frequencies merge: ε' ~ 30. A similar behavior is observed for σ. Here it is remarkable, that variable range hopping contributions, i.e. an increase of the ac-conductivity with increasing frequency, seem to be present already at 300 K, however, this mixes with the contact contribution. But we do not see a sharp, divergence-like anomaly in ε' as we would expect for ferroelectric (FE) transitions in the range from 2 to 300K. We measured P(E) at 2 K where the conductivity has decreased but we see no FE hysteresis. We also did dielectric pulse measurements (up-up-down-down-sequence, also known as PUND [34]). At low temperature, the samples behave like insulating paraelectrics, i.e. only the capacitive charging current, which decays exponentially after the switching of the electric field, can be seen. At higher temperature and room temperature they look like paraelectric plus conductivity (Contacts and/or VRH) indicated by the additional constant current density during the electric field pulse. But there are no indications of FE. (For that, the first up/down pulse should look significantly larger than the second reflecting the switched remnant polarization (see $BaTiO_3$)). But the structural polarity (setting in at the structural transition at higher temperature) is not

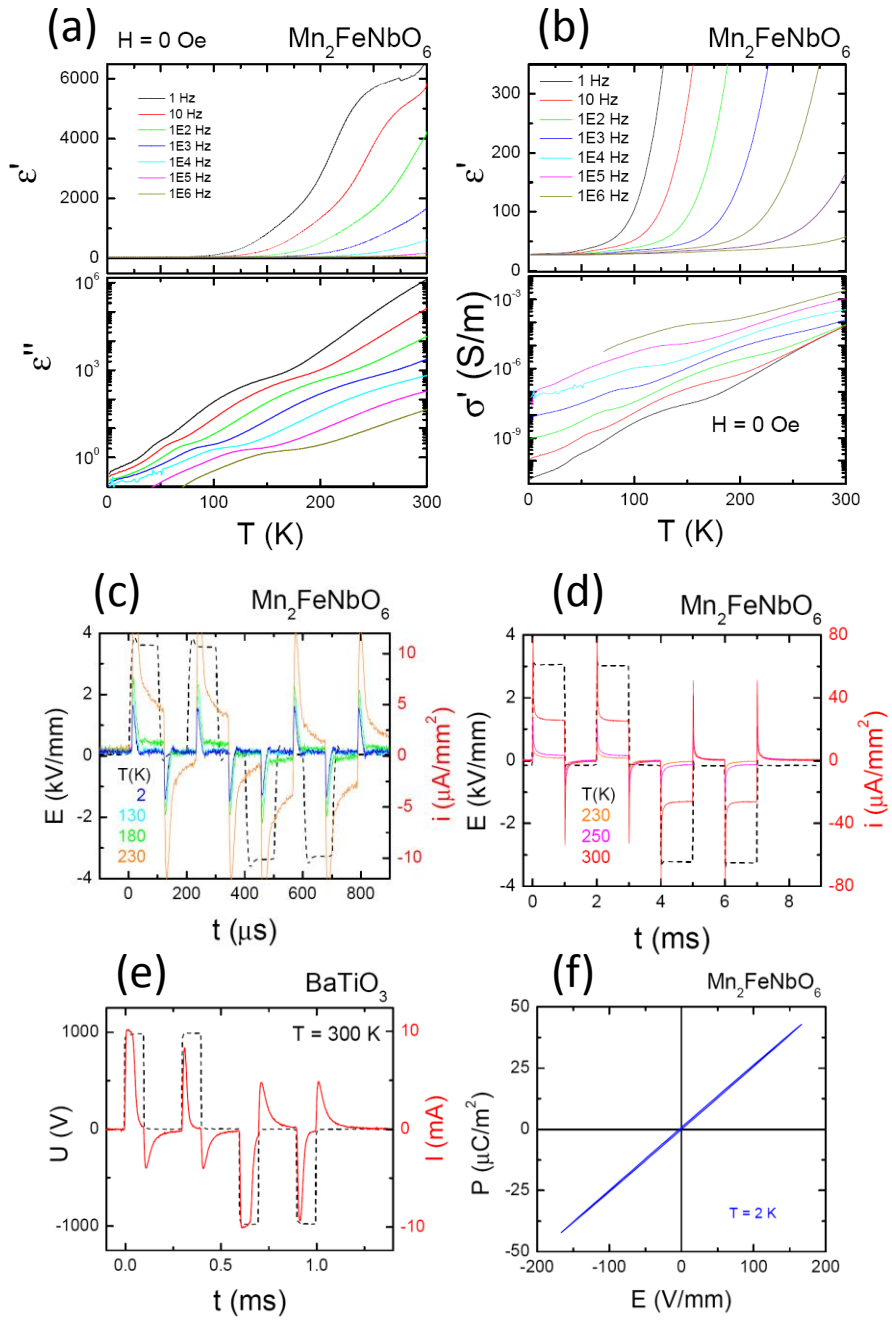

Fig. S9 Temperature dependence of the (a) dielectric permittivity ε' (top) and loss ε'' (bottom) as measured for frequency between 1 and10 MHz; and (b) enlarged dielectric permittivity ε' (below 300, top) and conductivity of Mn_2FeNbO_6 up to 300 K; Temperature dependent (c) long and (d) short time pulse dielectric measurements on Mn_2FeNbO_6 up to 300 K; (e) pulse dielectric data of $BaTiO_3$ at 300 K for comparison; and (f) P(E) loop of Mn_2FeNbO_6 measured at 2 K.

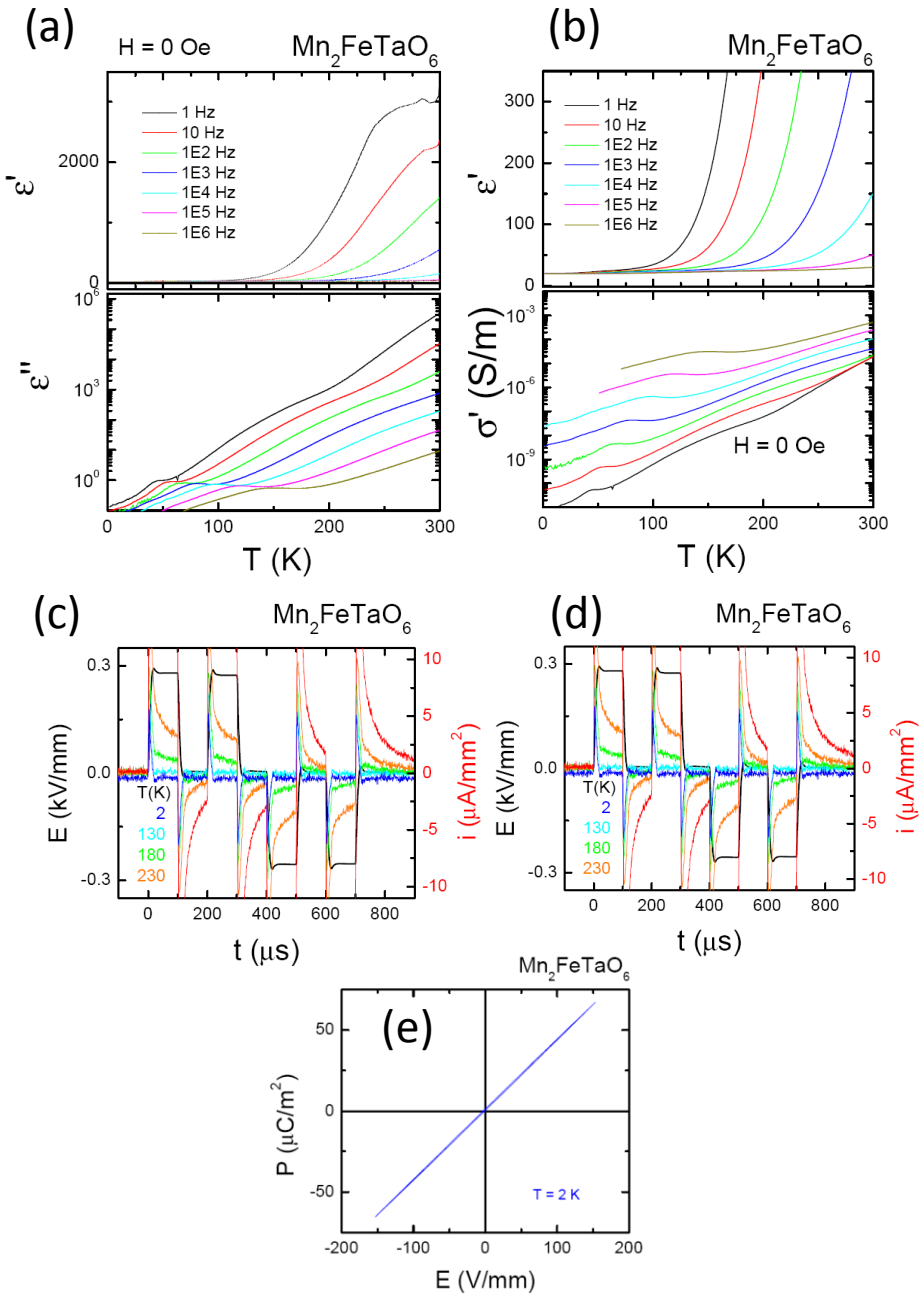

Fig. S10 Temperature dependence of the (a) dielectric permittivity ε' (top) and loss ε" (bottom) as measured for frequency between 1 and1 MHz; and (b) enlarged dielectric permittivity ε' (below 300, top) and conductivity of Mn_2FeTaO_6 up to 300 K; (c) 300 K long and (d) temperature dependent short time pulse dielectric measurements on Mn_2FeTaO_6; (e) P(E) loop of Mn_2FeTaO_6 measured at 2 K.

switchable by external fields - thus the material is polar but not ferroelectric. Pyroelectricity was found in the samples at lower temperature, where the samples are not too conductive.

References

1 Belik, A. A.; Furubayashi, T.; Yusa, H. & Takayama-Muromachi, E. *J. Am. Chem. Soc.* **133**, 9405-9412 (2011).

2 Li, M.-R.; *U*mut, A.; McMitchell, S. R. C.; Xu, Z.; Thomas, C. I.; Warren, J. E.; Giap, D. V.; Niu, H.; Wan, X.; Palgrave, R. G.; Schiffmann F.; Cora F.; Slater, B.; Burnett, T. L.; Cain, M. G.; Abakumov, A. M.; Tendeloo van, G.; Thomas, M. F.; Rosseinsky, M. J. & Claridge, J. B.. J. *Am. Chem. Soc.* **134**, 3737-3747. (2012).

3 Varga, T.; Kumar, A.; Vlahos, E.; Denev, S.; Park, M.; Hong, S.; Sanehira, T.; Wang, Y.; Fennie, C. J.; Streiffer, S. K.; Ke, X.; Schiffer, P.; Gopalan, V. & Mitchell, J. F. *Phys. Rev. Lett.* **103**, 047601 (2009).

4 Rohweder, U. & Müller-Buschbaum, H. *J. Less Common Met.* **138**, 79-86, (1988).

5 Sato, A. *J. Phys. Soc. Jpn.* **50**, 6 (1981).

6 Shannon, R. *Acta Crystallogr*. *A***32**, 751-767 (1976).

7 Lufaso, M. W. & Woodward, P. M. *Acta Crystallogr*. *B***57**, 725-738 (2001).

8 Coelho, A. *TOPAS-Academic, General Profile and Structure Analysis Software for Powder Diffraction Data*, version 4.1; http://www.topas-academic.net. (2007).

9 Mathieu, R.; Ivanov, S.; A., Bazuev,; G. V.; Hudl, M.; Lazor, P.; Solovyev, I. V. & Nordblad, P.. *Appl. Phys. Lett.* **98**, 202505 (2011).

10 Kurtz, S. K. & Perry, T. T. A *J. Appl. Phys.* **39**, 3798-3813 (1968).

11 Croft, M.; Sills, D.; Greeblatt, M.; Lee, C.; Cheong, S. W.; Ramanujachary, K. V. & Tran, D. *et al. Phys. Rev. B* **55**, 8726-8732 (1997).

12 Popov, G., Greenblatt, M. & Croft, M. *Phys Rev. B* **67**, 024406 (2003).

13 Mandal, T. K., Poltavets, V. V., Croft, M. & Greenblatt, M. S. *J. Solid State Chem.* **181**, 2325-2331 (2008).

14 Mandal, T. K.; Croft, M.; Hadermann, J.; Tendeloo van, G.; Stephens, P. W. & Greenblatt, M. *J. Mater. Chem.* **19**, 4382-4390 (2009).

15 Bune, R. O.; Lobanov, M. V.; Popov, G.; Greenblatt M.; Botez, C. E.; Stephens, P. W.; Croft, M.; Hardermann, J. & Tendeloo van, G.. Cr *Chem. Mater.* **18**, 2611-2617, (2006).

16 Zeng, Z., Fawcett, I. D., Greenblatt, M. & Croft, M. *Mater. Res. Bul.* **36**, 705-715, (2001).

17 Veith, G. M., Greenblatt, M., Croft, M. & Goodenough, J. B.. *Mater. Res. Bull.* **36**, 1521-1530 (2001).

18 Ramanujachary, K. V.; Lofland, S. E.; McCarroll, W. H.; Emge, T. J.; Greenblatt, M. & Croft. M. *J. Solid State Chem.* **164**, 60-70 (2002).

19 Veith, G. M.; Greenblatt, M.; Croft, M.; Ramanujachary, K. V.; Hattrick-Simpers, J.; Lofland, S. E. & Nowik, I. *Chem. Mater.* **17**, 2562-2567 (2005).

20 Veith, G. M.; Lobanov, M. V.; Emge, T. J.; Greenblatt, M.; Croft, M.; Stowasser, F.; Hadermann, J. & Tendelo van, G. *J. Mater. Chem.* **14**, 1623-1630 (2004).

21 Huang, Y.-H.; Croft, Mark.; Lehtimäki, M.; Karppinen, M. & Goodenough, J. B. *Chem. Mater.* **21**, 2319-2326 (2009).

22 Yang, T.; Perkisas, T.; Hadermann, J.; Croft, M.; Ignatov, A. & Greenblatt, M. *J.Solid State Chem.* **183**, 2689-2694 (2010).

23 Perdew, J. P.; Chevary, J. A.; Vosko, S. H.; Jackson, K. A.; Pederson, M. R. & Singh, D. J. *Phys. Rev. B* **46**, 6671 (1992)

24 Perdew, J. P.; Burke, K. & Ernzerhof, M. *Phys. Rev. Lett.* **77**, 3865 (1996).

25 Anisimov, V. I.; Zaanen, J. & Andersen, O. K. *Phys. Rev. B* **44**, 943 (1991).

26 Liechtenstein, A. I.; Anisimov, V. I. & Zaanen, J. *Phys. Rev. B* **52**, R5467 (1995).

27 Dudarev, S. L.; Bolton, G. A.; Savrasov, S. Y.; Humphreys, C. J. & Sutton, A. P. *Phys. Rev. B* **57**, 1505 (1998).

28 Kresse, G. & Hafner, J. *Phys. Rev. B* **47**, 558 (1993).

29 Kresse G. & Hafner, J. *Phys. Rev. B* **48**, 13115 (1993).

30 Kresse, G.& Hafner, J. *Phys. Rev. B* **49**, 14251 (1994).

31 Kresse, G. & Joubert, D. *Phys. Rev. B* **59**, 1758 (1999).

32 a) King- Smith, R. R. & Vanderbilt, D. Phys. Rev. B 47, 1651(1993); b) Vanderbilt, D. & King-Smith, R. D. Phys. Rev. B 48, 4442(1994).

33 Niermann, D.; Waschkowski, F.; de Groot, J.; Angst, M. & Hemberger, J. *Phys. Rev. Lett.* ***109****, 016405* (2012)

34 Scott, J. F. *Ferroelectric Memories*, Springer, Berlin, 2000, Chap. 6.

checkCIF/PLATON report

You have not supplied any structure factors. As a result the full set of tests cannot be run.

No syntax errors found. CIF dictionary Interpreting this report

Datablock: Mn2FeNbO6

```
Bond precision:  Mn- O = 0.0152 A        Wavelength=0.71073

Cell:            a=5.27403(5)     b=5.27403(5)     c=13.93381(18)
                 alpha=90         beta=90          gamma=120
Temperature:     298 K

                 Calculated                Reported
Volume           335.649(9)                335.649(8)
Space group      R 3 c                     R 3 c
Hall group       R 3 -2"c                  R 3 -2"c
Moiety formula   Fe Mn2 Nb O6              ?
Sum formula      Fe Mn2 Nb O6              Fe Mn2 Nb O6
Mr               354.64                    354.64
Dx,g cm-3        5.264                     0.000
Z                3                         0
Mu (mm-1)        11.132                    0.000
F000             495.0                     0.0
F000'            491.91
h,k,lmax
Nref
Tmin,Tmax
Tmin'

Correction method= Not given

Data completeness=                Theta(max)=

R(reflections)=                   wR2(reflections)=

S =                        Npar=
```

The following ALERTS were generated. Each ALERT has the format
test-name_ALERT_alert-type_alert-level.
Click on the hyperlinks for more details of the test.

Alert level A

```
PLAT043_ALERT_1_A Check Reported Molecular Weight ..............     354.64
PLAT091_ALERT_1_A No Wavelength found in CIF - 0.71073 Ang Assumed          ?
```

Alert level C

```
CRYSC01_ALERT_1_C No recognised colour has been given for crystal colour.
```

Alert level G

```
PLAT004_ALERT_5_G Info: Polymeric Structure Found with Dimension .          2
PLAT045_ALERT_1_G Calculated and Reported Z Differ by .....       0.00 Ratio
PLAT104_ALERT_1_G The Reported Crystal System is Inconsistent with       R3c
PLAT301_ALERT_3_G Note: Main Residue  Disorder ...............         17 Perc.
PLAT811_ALERT_5_G No ADDSYM Analysis: Too Many Excluded Atoms ....          !
PLAT980_ALERT_1_G No Anomalous Scattering Factors Found in CIF ...          ?
```

```
   2 ALERT level A = Most likely a serious problem - resolve or explain
   0 ALERT level B = A potentially serious problem, consider carefully
   1 ALERT level C = Check. Ensure it is not caused by an omission or oversight
   6 ALERT level G = General information/check it is not something unexpected

   6 ALERT type 1 CIF construction/syntax error, inconsistent or missing data
   0 ALERT type 2 Indicator that the structure model may be wrong or deficient
   1 ALERT type 3 Indicator that the structure quality may be low
   0 ALERT type 4 Improvement, methodology, query or suggestion
   2 ALERT type 5 Informative message, check
```

It is advisable to attempt to resolve as many as possible of the alerts in all categories. Often the minor alerts point to easily fixed oversights, errors and omissions in your CIF or refinement strategy, so attention to these fine details can be worthwhile. In order to resolve some of the more serious problems it may be necessary to carry out additional measurements or structure refinements. However, the purpose of your study may justify the reported deviations and the more serious of these should normally be commented upon in the discussion or experimental section of a paper or in the "special_details" fields of the CIF. checkCIF was carefully designed to identify outliers and unusual parameters, but every test has its limitations and alerts that are not important in a particular case may appear. Conversely, the absence of alerts does not guarantee there are no aspects of the results needing attention. It is up to the individual to critically assess their own results and, if necessary, seek expert advice.

Publication of your CIF in IUCr journals

A basic structural check has been run on your CIF. These basic checks will be run on all CIFs submitted for publication in IUCr journals (*Acta Crystallographica*, *Journal of Applied Crystallography*, *Journal of Synchrotron Radiation*); however, if you intend to submit to *Acta Crystallographica Section C* or *E*, you should make sure that full publication checks are run on the final version of your CIF prior to submission.

Publication of your CIF in other journals

Please refer to the *Notes for Authors* of the relevant journal for any special instructions relating to CIF submission.

PLATON version of 05/11/2012; check.def file version of 05/11/2012

Datablock Mn2FeNbO6 - ellipsoid plot

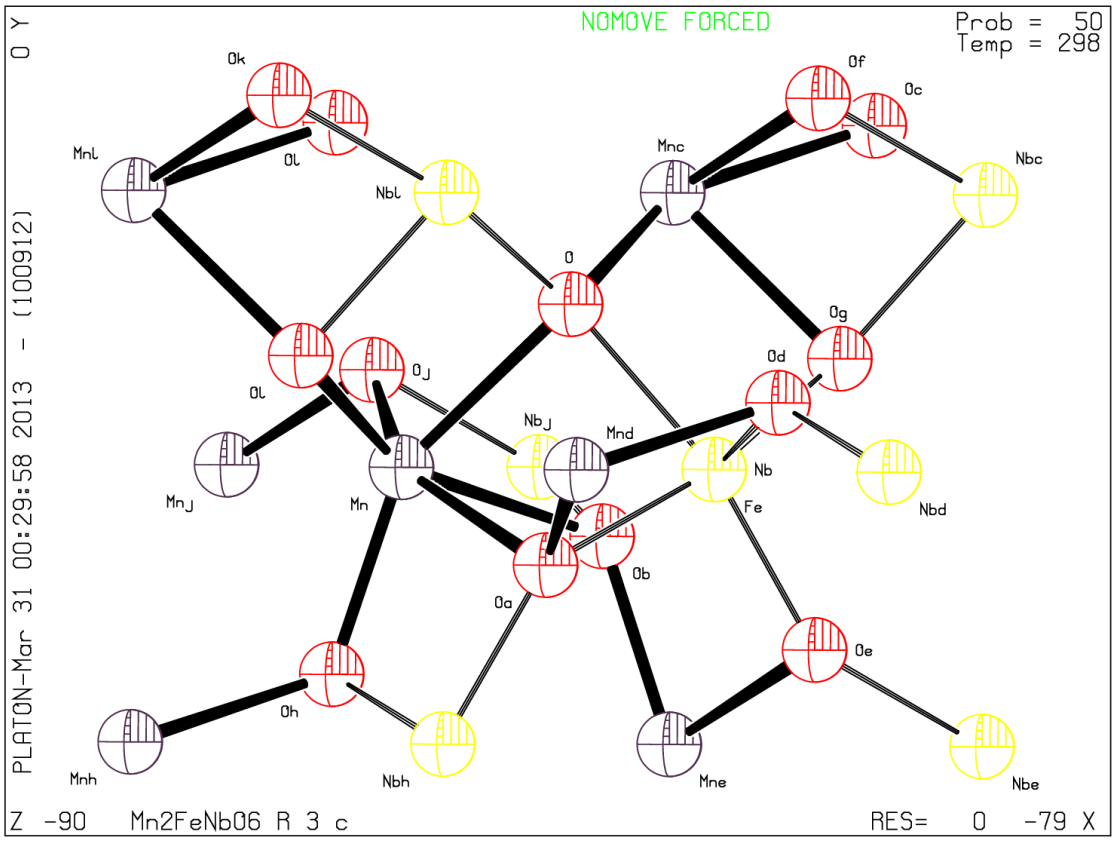

checkCIF/PLATON report

You have not supplied any structure factors. As a result the full set of tests cannot be run.

No syntax errors found. CIF dictionary Interpreting this report

Datablock: Mn2FeTaO6

```
Bond precision:  Mn- O = 0.0233 A        Wavelength=0.71073

Cell:            a=5.27208(10)     b=5.27208(10)     c=13.8892(3)
                 alpha=90          beta=90           gamma=120
Temperature:     298 K

                 Calculated                Reported
Volume           334.328(17)               334.330(10)
Space group      R 3 c                     R 3 c
Hall group       R 3 -2"c                  R 3 -2"c
Moiety formula   Fe Mn2 O6 Ta              ?
Sum formula      Fe Mn2 O6 Ta              Fe Mn2 O6 Ta
Mr               442.68                    442.68
Dx,g cm-3        6.596                     0.000
Z                3                         0
Mu (mm-1)        33.134                    0.000
F000             591.0                     0.0
F000'            592.51
h,k,lmax
Nref
Tmin,Tmax
Tmin'

Correction method= Not given

Data completeness=                Theta(max)=

R(reflections)=                   wR2(reflections)=

S =                        Npar=
```

The following ALERTS were generated. Each ALERT has the format
test-name_ALERT_alert-type_alert-level.
Click on the hyperlinks for more details of the test.

Alert level A

PLAT043_ALERT_1_A Check Reported Molecular Weight 442.68
PLAT091_ALERT_1_A No Wavelength found in CIF - 0.71073 Ang Assumed ?

Alert level C

```
CRYSC01_ALERT_1_C No recognised colour has been given for crystal colour.
```

Alert level G

```
PLAT004_ALERT_5_G Info: Polymeric Structure Found with Dimension .          2
PLAT045_ALERT_1_G Calculated and Reported Z Differ by .....       0.00 Ratio
PLAT152_ALERT_1_G The Supplied and Calc. Volume s.1. Differ by ...          7 Units
PLAT301_ALERT_3_G Note: Main Residue  Disorder ..................         17 Perc.
PLAT811_ALERT_5_G No ADDSYM Analysis: Too Many Excluded Atoms ....          !
PLAT980_ALERT_1_G No Anomalous Scattering Factors Found in CIF ...          ?
```

```
   2 ALERT level A = Most likely a serious problem - resolve or explain
   0 ALERT level B = A potentially serious problem, consider carefully
   1 ALERT level C = Check. Ensure it is not caused by an omission or oversight
   6 ALERT level G = General information/check it is not something unexpected

   6 ALERT type 1 CIF construction/syntax error, inconsistent or missing data
   0 ALERT type 2 Indicator that the structure model may be wrong or deficient
   1 ALERT type 3 Indicator that the structure quality may be low
   0 ALERT type 4 Improvement, methodology, query or suggestion
   2 ALERT type 5 Informative message, check
```

It is advisable to attempt to resolve as many as possible of the alerts in all categories. Often the minor alerts point to easily fixed oversights, errors and omissions in your CIF or refinement strategy, so attention to these fine details can be worthwhile. In order to resolve some of the more serious problems it may be necessary to carry out additional measurements or structure refinements. However, the purpose of your study may justify the reported deviations and the more serious of these should normally be commented upon in the discussion or experimental section of a paper or in the "special_details" fields of the CIF. checkCIF was carefully designed to identify outliers and unusual parameters, but every test has its limitations and alerts that are not important in a particular case may appear. Conversely, the absence of alerts does not guarantee there are no aspects of the results needing attention. It is up to the individual to critically assess their own results and, if necessary, seek expert advice.

Publication of your CIF in IUCr journals

A basic structural check has been run on your CIF. These basic checks will be run on all CIFs submitted for publication in IUCr journals (*Acta Crystallographica*, *Journal of Applied Crystallography*, *Journal of Synchrotron Radiation*); however, if you intend to submit to *Acta Crystallographica Section C* or *E*, you should make sure that full publication checks are run on the final version of your CIF prior to submission.

Publication of your CIF in other journals

Please refer to the *Notes for Authors* of the relevant journal for any special instructions relating to CIF submission.

PLATON version of 05/11/2012; check.def file version of 05/11/2012

Datablock Mn2FeTaO6 - ellipsoid plot